2010 IEEE International Conference on Robotics and Automation
Anchorage Convention District
May 3-8, 2010, Anchorage, Alaska, USA

Optimal Shape of a Snake Robot for Jumping

Keiichi Hoshino, Motoyasu Tanaka and Fumitoshi Matsuno

***Abstract*— In this paper, we discuss an optimal shape of the grounded part of a snake robot with passive wheels for jumping. First, we derive a relationship between constraint forces for the wheels and necessary friction forces, and propose a constraint force ellipse. Next, we introduce an evaluation index for the optimal shape of the grounded part (base part) of a snake robot using the constraint force ellipse. Finally, in order to demonstrate the validity of the optimal shape that minimizes the evolution index, simulations have been carried out.**

I. INTRODUCTION

A real snake is a simple structure without hands and legs, however it has various function [1]. There are many studies about mechanism and control of the snake robot which imitates a real snake. In these preceding studies, some locomotions of the snake, for example undulating locomotion [2], sinus-lifting motion [3] and winding motion [4] are studied. The real snakes can jump, however there is few study of jumping of the snake robots. Generally, it is said that the real snake does not have jumping power but it is known that adders and Jumping-pit vipers have high ability for jump. If a snake robot can jump, it is expected that the snake robot can expand the moving territory by adding ability of jumping. In addition, it helps to understand the jump function of the real snake. We consider jumping of snake robots with passive wheels in this study.

There are many and various studies about jumping robots. Most of these jumping robots have the legged mechanism. For example, a one-legged hopping robot was developed by Raibert et al. [5], jumping of a deformable soft robot is considered in [6] and a miniature jumping robot is studied in [7]. Ikeda et al. analyzed the jumping movements of the kangaroo and proposed a controller for running of one-legged robot with jumping [8]. And, Nakamura and Sugihara studied the jumping motion of humanoid robots [9]. Snake robots are different from these jumping robots, because of the presence of the anisotropic of friction of its body. Snake robots have characteristic that friction is small in the direction of its body line and is large in the vertical direction for its body line like the real snake. So, we need to discuss jump in consideration of this unique friction mechanism of the snake robot.

In this study, we define three processes of jumping, taking off, free-floating, and landing. It seems effective for jumping that the ground part of the snake robot does not slide before the taking off. The snake robot with passive wheels has anisotropic friction mechanism and friction force of the grounded part is depend on its shape.

K. Hoshino and M. Tanaka are with The University of Electro-Communications, Chofugaoka 1-5-1, Chofu, Tokyo, Japan, F. Matsuno is with Kyoto University, yoshidahonmachi, sakyoku, kyoto, kyoto, Japan matsuno@me.kyoto-u.ac.jp

In this paper, we propose a constrained force ellipse as a new evaluation index for calculating an optimal shape of the grounded part of the snake robot. To demonstrate the validity of the optimal shape simulations have been carried out.

II. MODEL

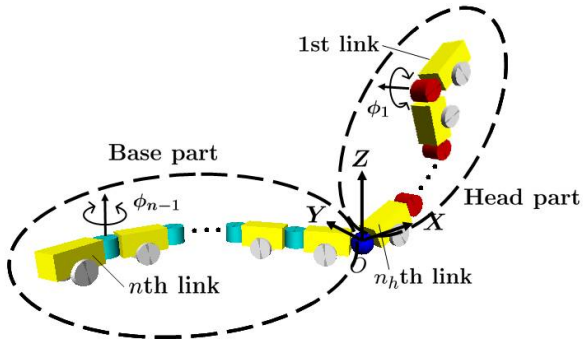

Fig. 1. A snake robot at the initial state and reference coordinate frame

In this paper, we consider an n-link snake robot and assume a wheel is placed at the center of gravity of each link. In the initial condition, the links from the 1st (head) to the n_h-th are lifted up, the links from the n_h+1-th to the n-th (tail) are grounded, and the robot does not have initial velocity as shown in Fig.1. In this situation, lifting links that are the links from the 1st to the n_h-th are called head part and grounded links that are the links from the n_h+1-th to the n-th are called base part. The total number of the base part is $n_b = n - n_h$.

Let us consider the jumping motion. Before taking off at least one link contacts to the ground. The time when all links do not contact to the ground and the robot is free-floating. It means that the robot takes off. After taking off, all joints of the snake robot are fixed. Then the robot falls down because of the gravitational force and touches the floor. It means that the robot lands. Each joint of the head part is a pitch rotational joint, each joint of the base part is a yaw rotational joint and joint between the head part and the base part is an universal joint. We define the joint between the head part and the base part as a connecting point. The position of the connecting point is set as the origin of the absolute coordinate system.

The direction of jump is set as the direction of X axis. For jumping only the head part is moved and all joints of the base part are rocked to suppress the slip during jumping movements. The snake robot should take an optimal shape of the base part for the effective jumping.

The reaction force $\boldsymbol{\lambda} = [\lambda_x, \lambda_y, \lambda_z]^T$ at the connecting point is generated by the movement of the head part. The Z axial component of $\boldsymbol{\lambda}$ is a reaction force from the floor. The slip motion of the robot will appear due to the force on XY plane $\boldsymbol{\lambda}_{xy} = [\lambda_x, \lambda_y]^T$. We consider an optimal shape of the base part which can diminished the slip of the body in order to realize an efficient jumping.

A. Base part model before taking off

We propose a constraint force ellipse which can evaluate the possibility of the slip due to the reaction force $\boldsymbol{\lambda}_{xy}$. Since the base part motion is limited on XY plane by introducing the assumption that the base part keeps contact with the floor before taking off, the base part can be regarded as a two dimensional n_b-link snake robot with passive wheels as shown in Fig.2.

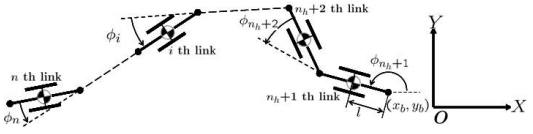

Fig. 2. Model of base part

We define that position of the connecting point is $\boldsymbol{w}_b = [x_b, y_b]^T$ with respect to the absolute coordinate system $O-XY$, the posture of the n_h+1-th link with respect to the absolute coordinate system is $\phi_{n_{h+1}}$, relative joint angles from n_h+2-th to n-th link is set as $\boldsymbol{\phi} = [\phi_{n_h+2}, \cdots, \phi_n]^T$ and $\boldsymbol{\phi}_b = [\phi_{n_{h+1}}, \boldsymbol{\phi}^T]$. Let us define $\boldsymbol{q}_b = [\boldsymbol{w}_b^T, \phi_{n_h+1}, \boldsymbol{\phi}_b^T]^T \in \mathbf{R}^{n_b+2}$ and the position of the center of the i-th link as $[x_i,\ y_i]^T$. We assume $\boldsymbol{w}_b = [0, 0]^T$ in the initial state. Let us define the posture of the i-th link with respect to the absolute coordinate system as $\theta_i = \phi_{n_h+1} + \sum_{j=n_h+2}^{i-1} \phi_j$. We assume that a passive wheel does not slide. The velocity constraint at the passive wheels of the i-th link ($i = n_h + 2, \cdots, n$) is expressed as,

$$\dot{x}_i \sin\theta_i - \dot{y}_i \cos\theta_i = 0. \tag{1}$$

Substituting the geometric relations

$$\begin{aligned} x_i &= x_b + 2l \sum_{j=n_h+2}^{i-1} \cos\theta_j + l\cos\theta_i \\ y_i &= y_b + 2l \sum_{j=n_h+2}^{i-1} \sin\theta_j + l\sin\theta_i. \end{aligned} \tag{2}$$

into (1) yields

$$A\dot{\boldsymbol{w}}_b = B\dot{\boldsymbol{\phi}}_b. \tag{3}$$

where

$$A = \begin{bmatrix} \sin\phi_{n_h+1} & -\cos\phi_{n_h+1} \\ \sin\theta_{n_h+2} & -\cos\theta_{n_h+2} \\ \vdots & \vdots \\ \sin\theta_n & -\cos\theta_n \end{bmatrix} \in \mathbf{R}^{n_b \times 2}$$

$$B = \begin{bmatrix} l & 0 & \cdots & 0 \\ b_{n_h+2,n_h+1} & l & \ddots & \vdots \\ \vdots & \ddots & \ddots & 0 \\ b_{n,n_h+1} & \cdots & b_{n,n-1} & l \end{bmatrix} \in \mathbf{R}^{n_b \times n_b}$$

$b_{i,j} = l + 2l\sum_{k=j}^{i-1} \cos(\sum_{s=k}^{i-1} \phi_s)$. We find that the matrix B is invertible.

Next, we consider a motion equation of the base part. Let us define the joint torque of the base part, so as to rock the every joint in the base part, as $\boldsymbol{\tau}_b = [\tau_{n_h+1}, \cdots, \tau_{n-1}]^T$, and the reaction force in the joint space corresponding to the constraint force $\boldsymbol{\lambda}_{xy}$ as $\boldsymbol{f} = [f_{n_h+1}, f_{n_h+2}, \cdots, f_n]^T$. A dynamic equation of the base part is given by

$$M\ddot{\boldsymbol{q}}_b + C\dot{\boldsymbol{q}}_b + J^T B^T \boldsymbol{f} = E\boldsymbol{\tau}_b + H\boldsymbol{\lambda}_{xy} \tag{4}$$

where, $M \in \mathbf{R}^{(n_b+2)\times(n_b+2)}$ is an inertia matrix, $C \in \mathbf{R}^{(n_b+2)\times(n_b+2)}$ is a matrix related to Coriolis and centrifugal force, $J = [-B^{-1}A, I_{n_b}] \in \mathbf{R}^{n_b\times(n_b+2)}$is a Jacobian matrix, $E = [O^T_{3\times(n_b-1)}, I_{n_b-1}]^T \in \mathbf{R}^{(n_b+2)\times(n_b-1)}$, $H = [I_2, O^T_{n_b\times 2}]^T \in \mathbf{R}^{n_b\times 2}$.

B. Head part model before taking off

As we assume the base part does not move before taking off, we can express position of the connecting point as $\boldsymbol{w}_b = [x_b, y_b, 0]^T$. Let ϕ_{n_h} be the absolute pitch posture of the n_h-th link, $\phi_i (i = 1, \cdots, n_h - 1)$ be the relative yaw angle of the n_h-th link, and $\tau_i (i = 1, \cdots, n_h - 1)$ be the joint torque of the head part as shown in Fig.3. Let us define $\boldsymbol{\phi}_h = [\phi_{n_h-1}, \phi_{n_h-2}, \cdots, \phi_1]^T$, $\boldsymbol{q}_h = [\boldsymbol{w}_b^T, \theta_{n_h}, \phi_{n_h}, \boldsymbol{\phi}_h^T]^T \in \mathbf{R}^{n_h+3}$,$\boldsymbol{\tau}_h = [\tau_{n_h}, \cdots, \tau_1]^T$. At the initial state we can assume $\boldsymbol{w}_b = [0, 0]^T, \theta_{n_h} = 0$.

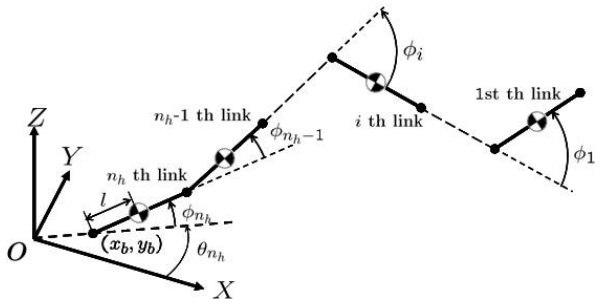

Fig. 3. Model of head part

A dynamic equation of the head part is expressed as

$$M_h\ddot{\boldsymbol{q}}_h + C_h = E_h\boldsymbol{\tau}_h \tag{5}$$

where, $M_h \in \mathbf{R}^{(n_h+3)\times(n_h+3)}$ is an inertia matrix, $C_h \in \mathbf{R}^{(n_h+3)}$ is a vector related to Coriolis, centrifugal force and gravity force, $E_h = [O^T_{3\times n_h}, I_{n_h}]^T \in \mathbf{R}^{(n_h+3)\times n_h}$.

III. CONSTRAINT FORCE ELLIPSE AND JUMPING MOTION CONTROL

In this paper, we propose a constraint force ellipse and derive a control law of jump by introducing the assumption that the base part of the robot does not move before taking off. Thus position of the connect point $w_b = [0, 0, 0]^T$ and the absolute yaw angle of the n_h-th link $\theta_{n_h} = 0$ are satisfied before taking off, and the motion of the head part is limited in XZ plane.

A. Constraint force ellipse

We assume that the base part does not slip and all joints of the base part are fixed, then we obtain $\ddot{\boldsymbol{q}}_b, \dot{\boldsymbol{q}}_b = \boldsymbol{0}$ and the motion equation of the base part is expressed as

$$J^T B^T \boldsymbol{f} = E\boldsymbol{\tau}_b + H\boldsymbol{\lambda}_{xy}. \tag{6}$$

Multiplying $[I_2, (B^{-1}A)^T]$ to the both side of (6) gives

$$\boldsymbol{\lambda}_{xy} = -[I_2, (B^{-1}A)^T]E\boldsymbol{\tau}_b. \tag{7}$$

Substituting (7) into (6) yields

$$\begin{aligned} J^T B^T \boldsymbol{f} &= [O_{n_b\times 2}, J^T]E\boldsymbol{\tau}_b \\ and\ \boldsymbol{\tau}_b &= ([O_{n_b\times 2}, B^{-T}]E)^\dagger \boldsymbol{f} \end{aligned} \tag{8}$$

where $Q^\dagger$ implies a pseudo-inverse matrix of the matrix Q. By substituting (8) into (7) we obtain

$$\boldsymbol{\lambda}_{xy} = -[I_2, (B^{-1}A)^T]E([O_{n_b\times 2}, B^{-T}]E)^\dagger \boldsymbol{f}. \tag{9}$$

The constraint force $\boldsymbol{f}$ is limited by maximum friction force between a wheel and an environment. By defining maximum sidling friction force of the i-th link as f_{imax} and $\boldsymbol{\lambda}_{xy}$ is rewritten as the following form

$$\boldsymbol{\lambda}_{xy} = PN\hat{\boldsymbol{f}} \tag{10}$$

where

$$\begin{aligned} P &= -[I_2, (B^{-1}A)^T]E([O_{n_b\times 2}, B^{-T}]E)^\dagger \\ N &= \mathrm{diag}(f_{n_h+1max}, f_{n_h+2max}, \cdots, f_{nmax},) \\ \hat{\boldsymbol{f}} &= \frac{\boldsymbol{f}}{||\boldsymbol{f}||},\ (\parallel \hat{\boldsymbol{f}} \parallel = 1). \end{aligned}$$

Based on the singular value decomposition of PN, we obtain an ellipse in XY plane as shown in Fig.4. Let us define singular values σ_l, σ_s and an orthonormal matrix $U = [\boldsymbol{u}_l, \boldsymbol{u}_s]$. Main axes of the ellipse are $\sigma_l\boldsymbol{u}_l$ and $\sigma_s\boldsymbol{u}_s$. $\sigma_l\boldsymbol{u}_l$ expresses a long axis of the ellipse and $\sigma_s\boldsymbol{u}_s$ expresses a short axis of the ellipse. In addition, the direction of u_l of the ellipse implies the direction that the robot can reinforce the largest disturbance force at the connecting point. The ellipse is called the constraint force ellipse. In this study, we decide the posture of the robot ϕ_{n_h+1} in such a way as to conform the direction of jumping, namely the long axis of the constraint force ellipse is set as the same direction as X axis by adjusting the posture of the robot as shown in Fig.5. Additionally, let us define the angle Θ_r between the vector of the long axis of the ellipse and the line connecting the center of gravity of the base part and the connecting point as shown in Fig.6. If Θ_r is large, the robot easily slipes and a rotational motion will be generated by the constraint force λ_{xy}.

B. Cost function

We calculate σ_l and Θ_r for each considering base part shape and the maximum values σ_{lmax} and Θ_{rmax}. Let us define the following formula as an evaluation index of slipping of the robot.

$$V = a(1 - \frac{\sigma_l}{\sigma_{l\max}}) + b\frac{\Theta_r}{\Theta_{r\max}}. \tag{11}$$

where a and b are positive constants. The first term and the second term of the right hand side of (11) are related to the translational slip and the rotational slip, respectively. We derive an optimal shape of the base part of the robot so as to minimize the cost function V.

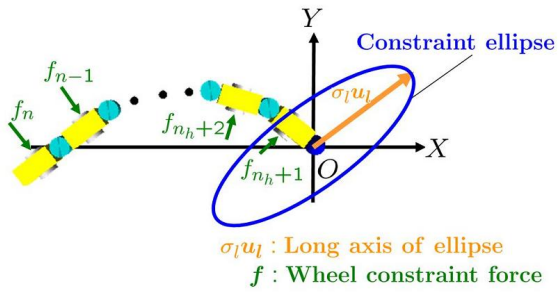

Fig. 4. A constraint ellipse

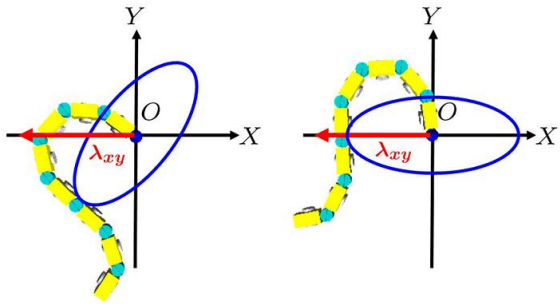

Fig. 5. Determination of attitude of base part considering jumping direction

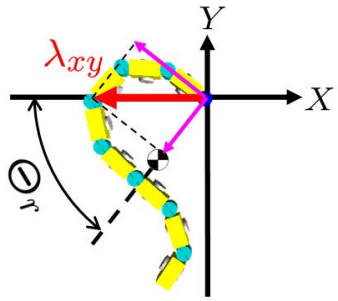

Fig. 6. Definition of Θ_r

C. Jumping motion of head part

As we assume that the base part of the robot does not slip, the head part of the robot is regarded as a serial link robot that is fixed at the ground [10]. Let us define a subvector of $\boldsymbol{q}_h$ as $\boldsymbol{q}_{hl} = [\phi_{n_h}, \boldsymbol{\phi}_h^T]^T \in \mathbf{R}^{n_h}$. The related motion equation of the head part (5) is obtained by

$$M_{hl}\ddot{\boldsymbol{q}}_{hl} + C_{hl} = \boldsymbol{\tau}_h \tag{12}$$

where $M_{hl} = E_h^T M_h E_h, C_{hl} = E_h^T C_h$. In this study, we derive a control law of the head part for the jumping motion on the basis of this model. In the free-floating period the robot rocks all joints of it. The jumping mechanism in this paper is as follows. At the initial condition at t_o the robot does not have an initial velocity. The Z axis velocity of the center of gravity of the head part increases by the motion of the head part. And the joints of the head part are controlled to decrease the velocity to 0 at t_e. The velocity of the robot becomes 0, however it has a linear momentum. Then the robot starts to take off. To realize this jumping motion we need to control the velocity of the center of gravity of the head part as desired value. We design an controller based on the model of the head part and a trajectory tracking controller. We define $\boldsymbol{r} = [x_g, z_g]^T$ is the position of the center of gravity, $\boldsymbol{r}_d = [x_{gd}, z_{gd}]^T$ is the desired position of $\boldsymbol{r}$, $J_r(\boldsymbol{q}_{hl})$ is a Jacobi matrix, $J_r^*(\boldsymbol{q}_{hl}) = J_r^T(J_r J_r^T)^{-1}$ is a pseudo-inverse matrix of the Jacobi matrix J_r. We set an input torque as

$$\boldsymbol{\tau}_h = C_{hl} + M_{hl} J_r^*(-\dot{J}_r \dot{\boldsymbol{q}}_{hl} + \ddot{\boldsymbol{r}}_d - K_d \dot{\boldsymbol{e}} - K_p \boldsymbol{e}) \tag{13}$$

so as to acheive the convergence of the acceleration of the center of gravity to the desired value, where $\boldsymbol{e} = \boldsymbol{r} - \boldsymbol{r}_d$ is an error vector, $K_d = \mathrm{diag}\,(K_{d1}, K_{d2}), K_p = \mathrm{diag}\,(K_{p1}, K_{p2})$.

We explain a condition of the take off to design an desired accelerate trajectory. We define that the total mass of the head part is m_h, acceleration of the center of gravity $[\ddot{x}_g, \ddot{z}_g]^T$, and the ground reaction force $\lambda_z(t)$. As the base part does not move, the robot's momentum at the take off time $t = t_e$ is $[m_h \dot{x}_g(t_e), m_h \dot{z}_g(t_e)]^T$ and we obtain the motion

$$\lambda_z(t) = m_h \ddot{z}_g + m_h g. \tag{14}$$

As $\ddot{z}_g = 0$ at the take off time $t = t_e$, from (14) we obtain

$$\lambda_z(t_e) = m_h g. \tag{15}$$

The force acting on the robot at $t = t_e$ conforms with its initial state and it has a momentum $m_h[\dot{x}_g(t_e), \dot{z}_g(t_e)]$. The direction of the robot at the take off is equivalent to the direction of the momentum vector. The elevation angle θ_e of the jumping is given as

$$\theta_e = \tan^{-1} \frac{\dot{z}_g(t_e)}{\dot{x}_g(t_e)}. \tag{16}$$

For example, if $\dot{x}_g(t_e) = 0$ the robot jumps vertically and if $\dot{x}_g(t_e) = \dot{z}_g(t_e)$ the robot jumps to the direction with the elevation angle 45[deg]. In this study, we define $\ddot{\boldsymbol{r}}_d = [a_1 \sin(\pi t/t_e), a_2 \sin(\pi t/t_e)]^T$ so as to satisfy $\theta_e = 45$[deg].

IV. SIMULATION

We consider an optimal shape of the base part of the robot for jump by minimizing evaluation function (11) and demonstrate the validity of it by simulations.

A. Derivation of optimal shape of the base part

In this simulation, we consider a 16-link snake robot where $n_h = 8, n_b = 8$ for calculating an optimal shape of the robot. We set the link mass $m = 0.5$[kg], the link length $2l = 0.15$[m], the coefficient of the static friction between wheels and ground as $\mu = 0.5$. We assume that reaction force λ_z at the connecting point concentrates to the $n_h + 1$-th link and the shape of the base part is set as a discretized serpenoid curve. Serpenoid curve is snake's winding curve. If the length of the link and number of links are known, the serpenoid curve is determined by the winding angle α and the cycle T as shown in Fig.7. When we change α and T in $1 \leq \alpha \leq 90$[deg],$0.5 \leq T \leq 2.5$, the obtained σ_l, Θ_r are shown in Fig.8(a) and (b). In the case $a = b = 1$, we find that the shape corresponding to $\alpha = 90, T = 0.79$ is optimal for jumping. To demonstrate the validity of the optimal shape dynamic simulations are carried out. We compare the motions of the center of gravity p_g of the base part of the robot for the optimal base part shape (A) and the worst base part shape (B) $\alpha = 1, T = 2.48$, in the case of $a = b = 1$. We also detain sub optimal shapes for the case (C) where $a = 0, b = 1$ and the case (D) where $a = 1, b = 0$. We also compare the motions of the optimal shape, the sub optimal shape (C) $\alpha = 81, T = 0.96$ and the other side optimal shape (D) $\alpha = 81, T = 0.69$. In addition, we define $O_G - X_G Y_B$ as a coordinate system translated $O - XY$ to the initial position O_G of the center of gravity of the base part $\boldsymbol{p}_g$ at $t = 0$ (Fig.9).

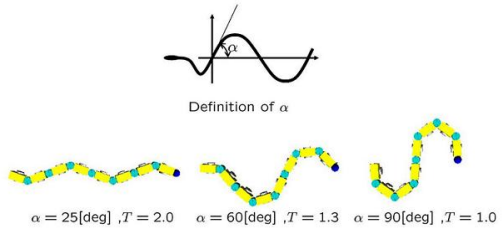

Fig. 7. Definition of α and T

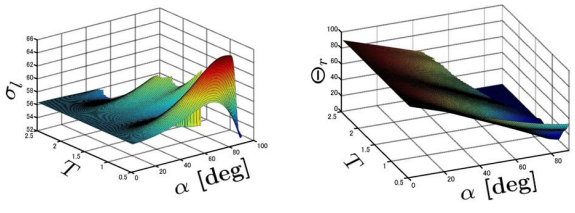

(a) σ_l (b) Θ_r

Fig. 8. Plots of $\sigma_l(T, \alpha)$ and $\Theta_r(T, \alpha)$

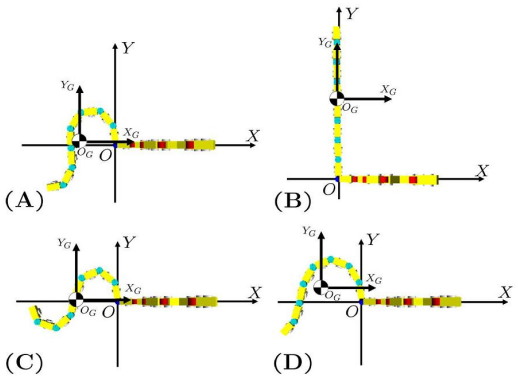

Fig. 9. Shapes of base part

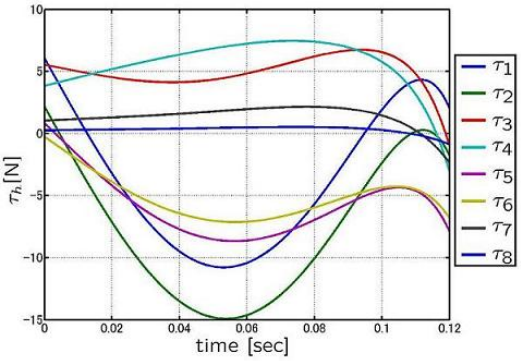

Fig. 11. Input torque of head part

B. Jumping simulation

In this simulation we demonstrate the validity of the obtained optimal shape of the snake robot in the previous section by dynamic simulations. The initial condition of the head part is set as $\boldsymbol{q}_h = [0.524, 0.0, 1.57, -1.22, -1.57, 1.57, 1.22, -1.57]^T$ and the target trajectory is given as $\ddot{\boldsymbol{r}}_d = [a_1 \sin(\pi t/t_e),\ a_2 \sin(\pi t/t_e)]^T$, where $a_1 = a_2 = 20$[m/s^2],$t_e = 0.12$[sec] as shown in Fig.10.

Fig.11 shows the input torque $\boldsymbol{\tau}_h$ of the head part. Fig.12 shows reaction force $|\boldsymbol{\lambda}_{xy}|, \lambda_z$ and generated friction force $\mu\lambda_z$ of the $n_h + 1$-th link. From Fig.12 we find that the friction force $\mu\lambda_z$ of the n_{h+1}-th link is smaller than $|\boldsymbol{\lambda}_{xy}|$ from $t = 0.02$[s] to $t = 0.1$[s] ($\mu\lambda_z \leq |\lambda_{xy}|,\ 0.02 \leq t \leq 0.1$). In this period the friction forces which are generated by the passive wheels contribute not to slip the robot body.

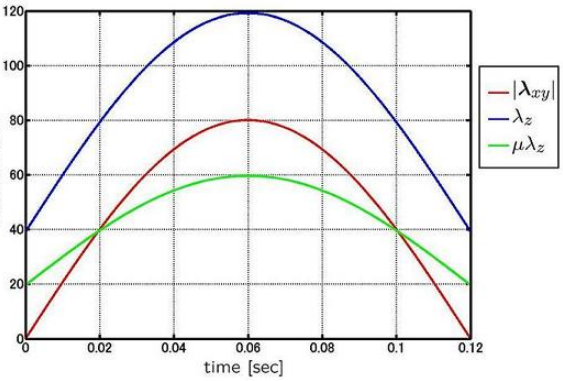

Fig. 12. Floor reaction force and frictional force

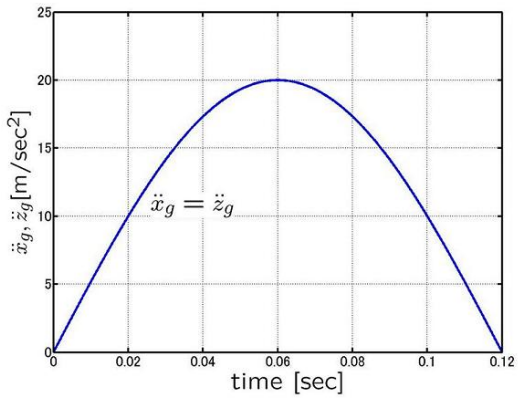

Fig. 10. Desired trajectory of acceleration of $\boldsymbol{r}$

The trajectories of the center of gravity $\boldsymbol{p}_g$ of the base part of the robot for the cases (A), (B), (C), (D) are shown in Fig.13. Fig.14 shows an enlargement of Fig.13 at the neighborhood of the origin O_G. In Fig.13, the blue circle and the green circle represent th positions of $\boldsymbol{p}_g$ at the taking off and the landing, respectively. In Fig.13, the blue solid line and the red solid line represent the trajectory of $\boldsymbol{p}_g$ from the initial time to the taking off time and the trajectory of $\boldsymbol{p}_g$ from the taking off time to the landing time, respectively. The blue solid line implies the slipping trajectory. Let us define d_x as the jumping distance and θ_x as the angle between X_G axis and the position vector of the landing point P_L as shown in Fig.15. TableI shows values of d_x and θ_x of the simulation results in the cases (A)-(D). In (B), the robot jumps backward. In (C), the slip distance is large and the jumping trajectory does not fit the jumping direction. And in (D), the slip distance not so large, while the jumping trajectory does not fit the jumping direction. In (A), the slip distance and the error of jumping direction are small and d_x is maximum in comparison with the others. Therefore, we can show the validity of the optimal shape of the base part of the wheeled snake robot for jumping and the evaluation function based on the proposed constraint force ellipse.

V. CONCLUDING REMARKS

In this paper we consider the optimal shape of the snake robot with passive wheels for the effective jumping. First, we propose the constraint force ellipse for evaluating the possibility of the slip considering the anisotropic friction mechanism of the snake robot. Next, we derive the optimal shape of the base part of the sake robot by minimizing the cost function based on the constraint force ellipse. Finally,

TABLE I
SIMULATION RESULT OF d_x AND θ_x

	(A)	(B)	(C)	(D)
d_x[mm]	112.3	-63.8	92.0	98.39
θ_x[deg]	1.546	168.5	-7.609	-5.256

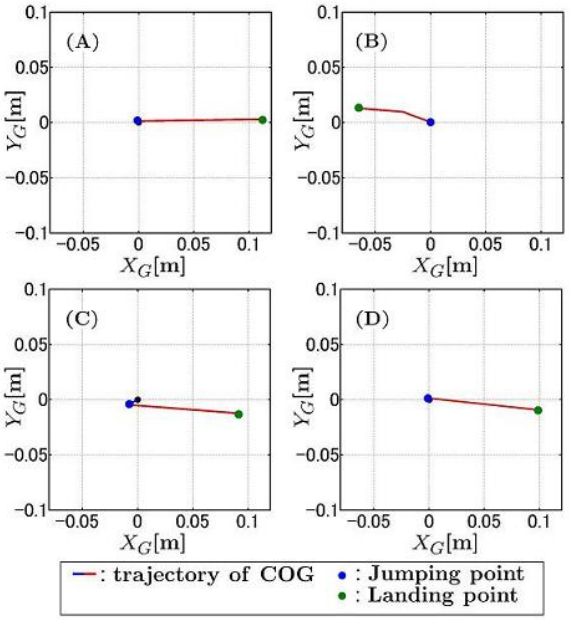

Fig. 13. Simulation results

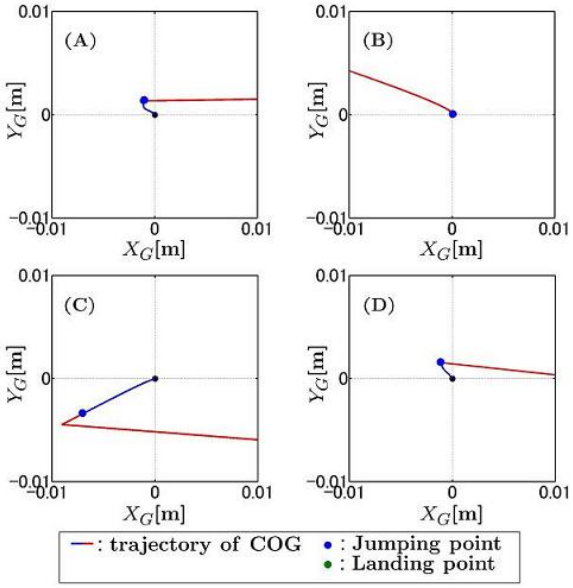

Fig. 14. Enlargement of Fig.13 at the neighborhood of O_G

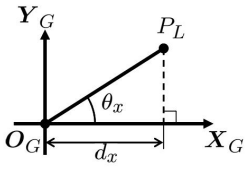

Fig. 15. Definition of d_x and θ_x

to demonstrate of the validity of the obtained optimal shape and the proposed cost function simulations are carried out.

In this paper the head part motion of the snake robot is given, then we consider the optimal shape of the base part. And the base part shape is determined based on the serpenoid curve. We introduce the assumption that the base part does not move before taking off. We should consider an optimal motion of the head part of the snake robot and an active motion of the base part for jumping.

REFERENCES

[1] S. Hirose, *Biologically Inspired Robots (Snake-like Locomotor and Manipulator)*, Oxford University Press, 1993.

[2] P. Prautsch and T. Mita, "Analysis and Control of a Gait of Snake Robot," *Proc. International Conference on Control Applications*, pp. 496-507, 1999.

[3] M. Tanaka and F. Matsuno, "A Study on Sinus-lifting Motion of a Snake Robot with Switching Constraints," *Proc.IEEE Int. Conf. on Robotics and Automation*, FrBll-1, 2009.

[4] K. Lipkin, I. Brown, A. Peck, H. Choset, J. Rembisz, P. Gianfortoni and A. Naaktgeboren, "Differentiable and Piecewise Differentiable Gaits for Snake Robots," *Proc. IEEE/RSJ Int. Conf. on Intelligent Robots and Systems*, pp. 1864-1869, 2007.

[5] M. H. Raibert, H. B. Brown, and M. Chepponis, "Experiments in Balance with a 3D One-legged Hopping Machine," *Int. J. Robot Res.*, 3 pp. 75-92, 1984.

[6] Y. Sugiyama, and S. Hirai, "Crawling and Jumping of Deformable Soft Robot," *Proc. IEEE/RSJ Int. Conf. on Intelligent Robots and Systems*, pp. 3276-3281, 2004.

[7] M. Kovac, M. Fuchs, A. Guignard, J. Zufferey, and D. Floreano, "A miniature 7g jumping robot," *IEEE International Conference on Robotics and Automation*, pp. 373-378, 2008.

[8] T. Ikeda, Y. Iwatani, K. Suse and T. Mita, "Analysis and Design of Running Robots in Touchdown Phase", *IEEE Conf. on Control Application*, pp. 496-501, 1999.

[9] T. Sugihara and Y. Nakamura,, "Contact Phase Invariant Control for Humanoid Robot based on Variable Impedant Inverted Pendulum Model", *IEEE International Conference on Robotics and Automation*, pp. 51-56, 2003.

[10] K. Arikawa and T. Mita, "Design of Multi-DOF Jumping Robot", *IEEE International Conference on Robotics and Automation*, pp. 3992-3997, 2002.